Journal of Electronic Materials (2025) 54:5792–5799
https://doi.org/10.1007/s11664-025-11908-5

ORIGINAL RESEARCH ARTICLE

Superconductivity in Tin Telluride Films Grown by Molecular Beam Epitaxy

Antonio Gonzalez[1] · Samuel J. Poage[1] · Bernardo Langa Jr.[2] · Deepak Sapkota[2] · Salva Salmani-Rezaie[3,4] · Shalinee Chikara[5] · Michael D. Williams[6] · David A. Muller[3,4] · Kasra Sardashti[2] · Kaveh Ahadi[1,7,8]

Received: 7 August 2024 / Accepted: 14 March 2025 / Published online: 29 April 2025

Abstract

The intersection of superconductivity and ferroelectricity hosts a wide range of exotic quantum phenomena. Here, we report on the observation of superconductivity in high-quality tin telluride films grown by molecular beam epitaxy. Unintentionally doped tin telluride undergoes a ferroelectric transition at ~100 K. The critical temperature of superconductivity increases monotonically with indium concentration. The critical field of superconductivity, however, does not follow the same behavior as critical temperature with indium concentration and exhibits a carrier-density-dependent violation of the Pauli limit. The electron–phonon coupling, according to the McMillan formula, exhibits a systematic enhancement with indium concentration, suggesting a potential violation of Bardeen–Cooper–Schrieffer (BCS) weak coupling at high indium concentrations.

Keywords Molecular beam epitaxy · tin telluride · superconductivity · topological insulator · ferroelectricity

Topologically nontrivial states in topological crystalline insulators (TCI) are protected by a lattice symmetry, as opposed to Z_2 topological insulators, in which time reversal symmetry protects these states.[1] Regardless of the nature of topological states, the combination of superconductivity and these states has the potential for topological superconductivity, which can enable fault-tolerant quantum computing.[2] Topological superconductivity emerge intrinsically or can be engineered at the interfaces between conventional, s-wave superconductors and topological insulators.[3] Furthermore, the combination of other emergent phenomena and superconductivity can give rise to exotic quantum phenomena.[4,5] For example, robust superconductivity with an enhanced critical temperature is observed when superconductivity emerges from a polar state.[6–8] Spin–orbit coupling (SOC) combined with inversion symmetry-breaking elements, i.e., Rashba SOC, in polar superconductors creates a helical spin configuration and enhances the superconductivity.[9] A combination of broken inversion symmetry and strong SOC also give rise to exotic superconducting states, including mixed-parity superconductivity,[10] topological Weyl superconductivity,[11] superconducting diode effect,[12] and upper critical field exceeding the Pauli limit.[13]

Tin telluride (SnTe) is a narrow-bandgap semiconductor (0.3 eV[14,15]) with a cubic rock salt crystal structure ($Fm\bar{3}m$) at room temperature.[16] It undergoes a ferroelectric transition to a rhombohedral structure ($R3m$) at ~100 K.[17–19] Tin telluride is a topological crystalline insulator in which topological surface states originate from the mirror symmetry with respect to the (110) planes.[20] The existence of gapless topological surface states was experimentally verified.[21,22] Tin telluride becomes superconducting upon doping.[23,24] Indium-doped bulk samples exhibit critical temperature (T_c)

✉ Kaveh Ahadi
ahadi.4@osu.edu

1 Department of Materials Science and Engineering, North Carolina State University, Raleigh, NC 27695, USA

2 Department of Physics and Astronomy, Clemson University, Clemson, SC 29634, USA

3 School of Applied and Engineering Physics, Cornell University, Ithaca, NY 14853, USA

4 Kavli Institute at Cornell for Nanoscale Science, Cornell University, Ithaca, NY 14853, USA

5 National High Magnetic Field Laboratory, Tallahassee, Fl 32310, USA

6 Department of Physics, Clark Atlanta University, Atlanta, GA 30314, USA

7 Department of Electrical and Computer Engineering, The Ohio State University, Columbus, OH 43210, USA

8 Department of Materials Science and Engineering, The Ohio State University, Columbus, OH 43210, USA

as high as ~4.5 K.[25] The solubility limit of indium in bulk tin telluride reaches ~50 at% at room temperature.[26] The mixed oxidation of indium (+1 and +3) creates amphoteric levels in tin telluride, which induces an anomalous dependence on indium concentration.[27] Molecular beam epitaxy (MBE)-grown layers recently demonstrated the emergence of versatile electronic states ranging from topologically nontrivial states and polar semimetals to superconductors.[28,29]

The superconductivity in tin telluride is an ideal platform for the experimental realization of polar superconductivity and nontrivial topology. Here, we report on high-quality molecular beam epitaxy growth and observation of a superconducting transition in indium-doped tin telluride. The critical temperature of superconductivity scales with indium concentration. We also observe the in-plane critical field violating the Pauli paramagnetic limit, depending on the indium density.

We used a chalcogenide MBE system (GEN 930) to grow high-quality indium-doped tin telluride. The films were grown on BaF_2 (111) substrates. BaF_2 was chosen due to its minimal lattice and thermal expansion coefficient mismatch with IV-VI materials. BaF_2 has a cubic structure ($Fm\bar{3}m$) with a lattice constant of ~0.62 nm. The substrate temperature was maintained at 400 °C (thermocouple temperature) during the growth. The growth rate was roughly one monolayer per second, and the film thickness was kept at ~450 nm, corroborated by cross-sectional scanning transmission electron microscopy (STEM) images. We used a tellurium-rich tin telluride source (99.999 at%, American Elements) to account for tellurium desorption and dopants. The $\theta - 2\theta$ x-ray diffraction (XRD) scan and rocking curve results for the films around 222 reflection can be found in the supplementary materials (Figure S1). The out-of-plane lattice constant ($a_\perp$), extracted from XRD, decreases with increasing indium concentration. The rocking curve full width at half maximum (FWHM) is ~325 arcsec, suggesting the high crystalline quality of the grown films. We also used STEM to examine the film and interface structure. Cross-sectional specimens were prepared using the Thermo Fisher Scientific Helios G4 UX focused ion beam system. High-angle annular dark-field (HAADF) images were captured using the Thermo Fisher Scientific Spectra 300 X-CFEG instrument, running at 300 kV with a convergence angle of 30 mrad and a HAADF with an angular range of 60–200 mrad. Figure 1a shows a HAADF-STEM image of the SnTe film grown on a (111)-oriented BaF_2 single-crystal substrate. STEM samples were cut along the substrate's edge, which exhibits an 11-degree miscut relative to the primary crystallographic direction of $[1\bar{1}0]$. The magnified section of

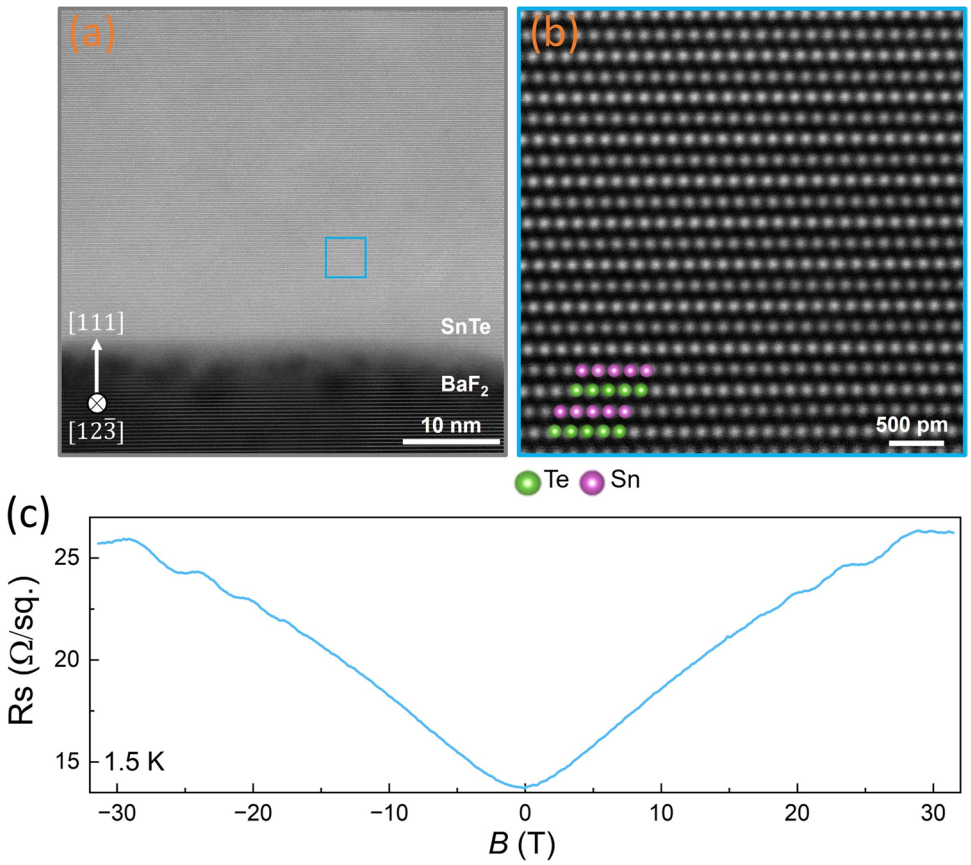

Fig. 1 Molecular beam epitaxy-grown tin telluride film on BaF_2 (111). (a) Cross-sectional HAADF-STEM image of the tin telluride film grown on BaF_2 (111). (b) Higher-magnification HAADF-STEM image of the tin telluride layer. (c) Longitudinal magnetoresistance measurement of unintentionally doped tin telluride at 1.5 K, exhibiting quantum oscillations.

Fig. 1b shows alternating layers of tellurium (brighter) and tin (darker) columns. Figure 1c shows the magnetoresistance measurement for the unintentionally doped sample carried out at 1.5 K. The observed quantum oscillations suggest high quality of the grown films. The charge carriers in the unintentionally doped films are due to point defects commonly observed in IV-VI semiconductors.[30] We controlled the indium concentration in the films using the indium cell temperature. Secondary ion mass spectroscopy (SIMS) indicates incorporation of the indium in the films (Figure S2). SIMS also confirms that the indium-to-tin ratio in the grown tin telluride scales with the indium cell temperature. The indium concentration profile, however, exhibits an upturn near the surface of the films with higher indium concentration. The substantial diffusion of indium and its exothermic substitutional doping at temperatures as low as room temperature was previously reported in PbTe.[31,32] Here, we observe indium migration towards the surface in highly doped films, which combined with favorable formation energy of InTe may explain the SIMS indium concentration profile in different samples.

Magneto-transport measurements were performed using the van der Pauw configuration and measuring the differential resistance (i.e., dV/dI). The temperature-dependent magneto-transport measurements (except Fig. 1c) were carried out in a Teslatron refrigerator (Oxford Instruments) with a lock-in amplifier in alternating current (AC) mode with excitation current ranging from 1 μA to 10 μA. Measurements below 1.5 K (down to 270 mK) were carried out in the same system using a Heliox VT ^{3}He Probe. The magnetoresistance of the unintentionally doped film (Fig. 1c) was carried out at the National High Magnetic Fields Laboratory using a resistive magnet with a lock-in amplifier and an excitation current of 1 μA.

Figure 2 shows the normalized resistance with temperature. All samples demonstrate a sharp superconducting transition. The critical temperature of superconductivity, corresponding to 0.5 Rn, is 2.4 K, 1.3 K, 1.1 K, and 0.75 K for indium cell temperatures of 810°C, 790°C, 760°C, and 710°C, respectively. Figure S3 exhibits the superconducting temperature with respect to the indium cell temperature. We estimate the Bardeen–Cooper–Schrieffer (BCS) gap $\left(\Delta_{BCS} \approx 1.76 K_B T_C\right)$ to be 364 μeV, 194 μeV, 159 μeV, and 139 μeV for indium cell temperatures of 810°C, 790°C, 760°C, and 710°C, respectively. The critical temperature of superconductivity scales with the indium concentration. The SIMS results reveal an indium concentration as high as ~15 at% in the sample with 810°C cell temperature, which is well below the solubility limit.[26]

Figure 3 shows the superconducting transition with the in-plane applied magnetic field at different temperatures. The orbital upper critical field (H_{C2}) of superconductivity at 270 mK, corresponding to 0.9 Rn, is 3.2 T, 2.2 T, 2.2 T,

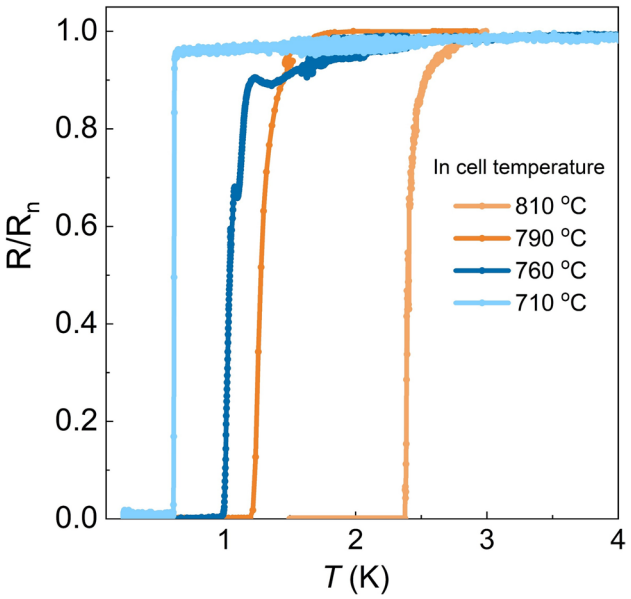

Fig. 2 Critical temperature of superconductivity with indium concentration in tin telluride films. Longitudinal normalized resistance (R/Rn, where Rn is the normal state resistance) of tin telluride films grown on BaF_2 (111) with temperature.

and 1.2 T for indium cell temperatures of 810°C, 790°C, 760°C, and 710°C, respectively. In the absence of spin–orbit interaction, there are two mechanisms by which an applied magnetic field can suppress superconductivity. One is the diamagnetic response related to the action of the field on the orbital motion of electrons forming a Cooper pair. Here, the Ginzburg–Landau coherence length($\xi_{GL} = \sqrt{\phi_o/2\pi H_{C2}}$, where ϕ_o is magnetic quantum flux) using the measured orbital upper critical field is 10 nm, 12 nm, 12 nm, and 17 nm for indium cell temperatures of 810°C, 790°C, 760°C, and 710°C, respectively, which are well below the thickness of the film, suggesting a three-dimensional superconductivity. The second mechanism is the paramagnetic response associated with the Zeeman splitting of the states with opposite spin, giving rise to the Pauli limit ($H_P \approx \Delta/\sqrt{2}\mu_B$, assuming a g-factor of 2 and weakly coupled superconductivity). We note that the measured orbital upper critical fields at 270 mK are near the Pauli limit, which we estimate to be 4.5 T, 2.4 T, 1.9 T, and 1.4 T for indium cell temperatures of 810°C, 790°C, 760°C, and 710°C, respectively.

A resistance upturn is observed prior to the superconducting transition upon a decrease in the field in higher indium concentrations at lower temperatures (Fig. 3a and b). Granular superconductors have exhibited similar behavior, where superconducting puddles form first.[33,34] Furthermore, an anisotropic resistance upturn prior to the superconducting transition has recently been reported.[13] Here, the resistance upturn could be due to pre-formed Cooper pairs in which

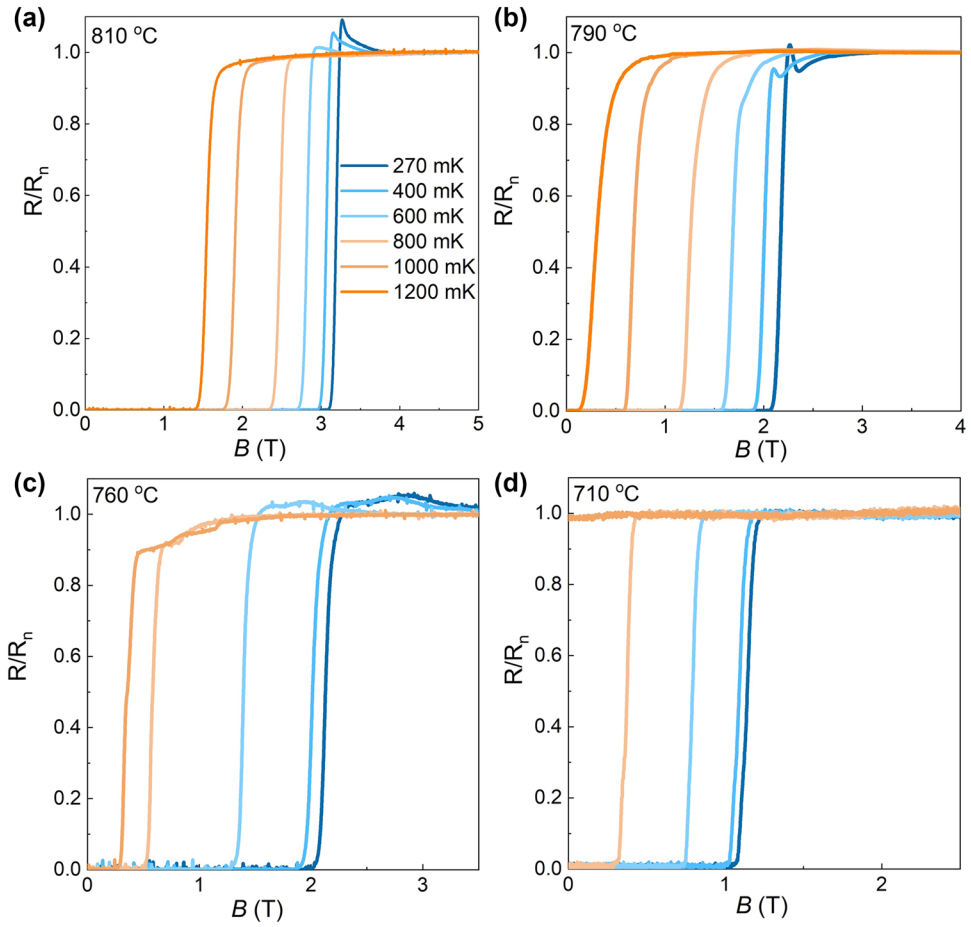

Fig. 3 In-plane critical field of superconductivity with indium concentration in tin telluride films. Longitudinal normalized resistance (R/Rn, where Rn is the normal state resistance) of tin telluride films grown on BaF_2 (111) with an in-plane magnetic field at various temperatures.

gapped-out quasiparticles disrupt transport[35] before global superconductivity prevails at lower fields.

Figure 4 shows the in-plane upper critical field (H_{C2}) of superconductivity with temperature. The critical field results were fitted using a modified Ginzburg–Landau model $H_{C2}(T) = H_{C2}(0)(1-t)^{\alpha}$, where $H_{C2}(0)$ is the upper critical field at 0 K and $t = T/T_C$. The temperature dependence of the critical field as described by Ginzburg–Landau theory predicts a linear relationship ($\alpha = 1$). The in-plane critical field in a thin film, however, can exhibit a square root characteristic ($\alpha = 0.5$), introduced by Tinkham.[36] Here, the highly doped sample's H_{C2} can be described by a linear fit, and lower-doped samples exhibit a mixed behavior ($0.5 < \alpha < 1$), which has been reported previously when the superconductor experiences a dimensional crossover.[13] The calculated coherence length matches previous reports[28,29] and is much smaller than the nominal film thickness. The superconducting layer thickness, however, might be challenging to estimate in the films due to the indium concentration gradient near the surface (Figure S2).

Table I summarizes the measured results for tin telluride films with different indium concentrations. The first important conclusion from these results is that the emergence of superconductivity in SnTe depends strongly on the indium concentration. The critical temperature and critical field of superconductivity scale with indium concentration. The in-plane critical field, however, becomes less sensitive to tin concentration around 10% SIMS indium concentration (cell temperatures of 760°C and 790°C). We also observe that the in-plane critical field reaches the Pauli paramagnetic limit in these films.

First, we discuss the effect of indium concentration on superconductivity. The insensitivity of the critical field to indium concentrations (760°C and 790°C indium cell temperatures) and a change in the critical field behavior with temperature raise the question of whether the nature of doping and superconductivity evolves with indium concentration in tin telluride. Substitution of tin (Sn^{2+}) with indium (In^{1+}) is expected to induce p-type carriers in tin telluride. The self-doped p-type (tin-deficient) tin telluride, however, shows different superconducting critical temperatures from those of indium-doped samples with similar carrier densities.[24,25,37,38] Furthermore, an anomalous change in doping character and superconductivity is reported with indium doping in bulk tin telluride at ~10 at.%.[27] The McMillan formula estimates the electron–phonon coupling constant (λ_{e-p}

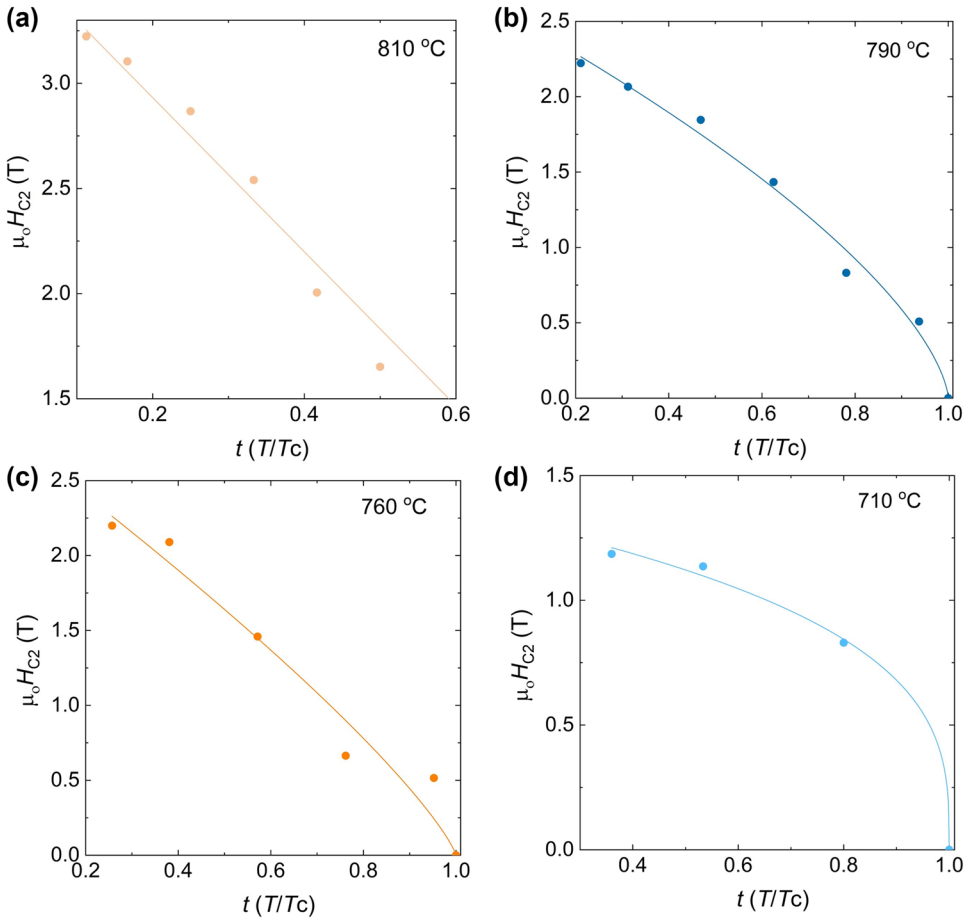

Fig. 4 In-plane critical field of superconductivity with temperature in tin telluride films. The results are in agreement with a modified Ginzburg–Landau model, $H_{C2}(T) = H_{C2}(0)(1-t)^{\alpha}$, where $H_{C2}(0)$ is the upper critical field at 0 K, $t = T/T_C$, and α is the dimensionality factor.

Table I Summary of superconducting and structural characterization of indium-doped tin telluride films grown by MBE

Indium cell temperature	$a_{\perp}(nm)$	T_C(K)	$\Delta_{BCS}(\mu eV)$	$H_{C2}(T)$	$\xi_{GL}(nm)$	$H_{C2}(0)/H_P$	λ_{e-p}
810°C	0.632	2.4	364	3.2	10	0.8	0.63
790°C	0.633	1.3	194	2.2	12	1.1	0.54
760°C	0.633	1.1	159	2.2	12	1.5	0.52
710°C	0.634	0.75	139	1.2	17	1.0	0.49

Values of lattice constant ($a_{\perp}$), critical temperature of superconductivity (T_C, defined at 0.5*R*n), BCS superconducting gap $\left(\Delta_{BCS} \approx 1.76K_BT_C\right)$, in-plane critical field (H_{C2}, defined at 0.9*R*n), coherence length (ξ_{GL}), the critical field to Pauli limit ratio ($H_{C2}(0)/H_P$), and electron–phonon coupling constant (λ_{e-p}).

).[39] The electron–phonon coupling constant is a dimensionless measure of the strength of electron–phonon coupling. The weak-coupling BCS model is valid for $\lambda_{e-p} \ll 1$.

$$\lambda_{e-p} = \frac{1.04 + \mu^* \ln\left(\Theta_D/1.45T_c\right)}{(1-0.62\mu^*)\ln\left(\Theta_D/1.45T_c\right) - 1.04}$$

where μ^* accounts for the screened Coulomb repulsion. The Debye temperature (Θ_D) was measured for bulk indium-doped tin telluride, and ranged from 204 K for 5% indium to 162 K for 40% indium.[27] We used the measured critical temperature (*T*c), approximated the Debye temperature of 200 K for all samples, and made the common assumption of $\mu^* = 0.15$.[39] The electron–phonon coupling constant is 0.63, 0.54, 0.52, and 0.49 for indium cell temperatures of 810°C, 790°C, 760°C, and 710°C, respectively. The films studied here remain within the BCS weak coupling regime, but the observed enhancement of λ_{e-p} with indium suggests a potential violation of the weak-coupling superconductivity regime in highly doped tin telluride. We note that violation of the BCS weak coupling regime was reported in bulk $Sn_{0.6}In_{0.4}Te$.[27] Furthermore, the strongly coupled superconductivity requires a correction to the superconducting gap $(\Delta > 1.76K_BT_C)$[40] in highly doped samples.

Next, we discuss the in-plane critical field of superconductivity in this system. Here, the $\left(H_{C2}(0)/H_P\right)$ ratio is 0.8, 1.1, 1.5, and 1.0 for indium cell temperatures of 810°C, 790°C, 760°C, and 710°C, respectively (Figure S3), suggesting that the films are near a violation of the Pauli limit. In superconducting thin films, spin–orbit scattering randomizes the spins and reduces the polarizing effect of the magnetic field.[41] Furthermore, the Rashba spin–orbit effect can enhance the critical field up to $\sqrt{2}H_P$[9] due to a distinctive helical spin configuration. The measured $H_{C2}(0)/H_P$ ratio, however, is smaller than that of other polar superconductors, $SrTiO_3$ (>4)[42] and $KTaO_3$ (>8).[43] The enhanced critical field of superconductivity in these material systems is attributed to the formation of quasiparticles with extraordinary resilience against the magnetic field, spin-orbit scattering, and mixed parity.[43] The orbital character of charge transport in tin telluride (*p*-orbital), however, is different from that in $SrTiO_3$ and $KTaO_3$ (*d*-orbital), which could explain the observed discrepancy in the $H_{C2}(0)/H_P$ ratio. Here, the spin–orbit scattering and/or Rashba spin–orbit coupling can potentially explain the enhanced critical field.

In summary, our results, in particular the dopant density dependence of the critical field and nature of superconductivity, should be of interest for proposals testing different models that relate superconductivity to a polar state.[44–50] Independently of the specific mechanism, the results point to opportunities to tune the critical field and the nature of pairing, and to search for new superconducting material systems that are in proximity to a polar instability. We stress that our findings warrant further study of superconductivity at the intersection of topologically nontrivial states and ferroelectricity.

Supplementary Information The online version contains supplementary material available at https://doi.org/10.1007/s11664-025-11908-5.

Acknowledgments SJP was supported by the U.S. National Science Foundation (NSF) under Grant DMR-2408890. KS and BL acknowledge funding from the U.S. National Science Foundation (NSF) under Grant 2137776. This work made use of a Helios focused ion beam scanning electron microscope supported by the NSF (Grant DMR-1539918) and the Cornell Center for Materials Research (CCMR) Shared Facilities, which are supported through the NSF MRSEC Program (Grant DMR-1719875). MDW also acknowledges support from National Science Foundation PREM Award no. 2122147. A portion of this work was performed at the National High Magnetic Field Laboratory, which is supported by National Science Foundation Cooperative Agreement DMR-2128556 and the State of Florida. AG and SJP acknowledge assistance from A. Al-Tawhid in growth experiments. BL thanks F. X. Duffy for his assistance in low-temperature experiments. KA acknowledges discussions with M. N. Gastiasoro.

Funding National Science Foundation, DMR-2408890, Kaveh Ahadi.

Data Availability The data that support the findings of this study are available in the article and its Supporting Information. Raw data can be obtained from the corresponding author upon request.

Conflict of interest The authors declare that they have no conflict of interest.

References

1. L. Fu, Topological crystalline insulators. *Phys. Rev. Lett.* 106(10), 106802 (2011). https://doi.org/10.1103/PhysRevLett.106.106802.
2. A. Yu Kitaev, Unpaired Majorana fermions in quantum wires. *Phys. Usp.* 44(10S), 131–136 (2001). https://doi.org/10.1070/1063-7869/44/10S/S29.
3. L. Fu and C.L. Kane, Superconducting proximity effect and majorana fermions at the surface of a topological insulator. *Phys. Rev. Lett.* 100(9), 096407 (2008). https://doi.org/10.1103/PhysRevLett.100.096407.
4. S.S. Saxena, P. Agarwal, K. Ahilan, F.M. Grosche, R.K.W. Haselwimmer, M.J. Steiner, E. Pugh, I.R. Walker, S.R. Julian, P. Monthoux, G.G. Lonzarich, A. Huxley, I. Sheikin, D. Braithwaite and J. Flouquet, Superconductivity on the border of itinerant-electron ferromagnetism in UGe_2. *Nature* 406(6796), 587–592 (2000). https://doi.org/10.1038/35020500.
5. S. Kanasugi and Y. Yanase, Spin-orbit-coupled ferroelectric superconductivity. *Phys. Rev. B* 98(2), 024521 (2018). https://doi.org/10.1103/PhysRevB.98.024521.
6. R. Russell, N. Ratcliff, K. Ahadi, L. Dong, S. Stemmer and J.W. Harter, Ferroelectric enhancement of superconductivity in compressively strained $SrTiO_3$ films. *Phys. Rev. Mater.* 3(9), 091401 (2019). https://doi.org/10.1103/PhysRevMaterials.3.091401.
7. K. Ahadi, L. Galletti, Y. Li, S. Salmani-Rezaie, W. Wu and S. Stemmer, Enhancing superconductivity in $SrTiO_3$ films with strain. *Sci. Adv.* 5(4), eaaw0120 (2019). https://doi.org/10.1126/sciadv.aaw0120.
8. S. Salmani-Rezaie, K. Ahadi and S. Stemmer, Polar Nanodomains in a Ferroelectric Superconductor. *Nano Lett.* 20(9), 6542–6547 (2020). https://doi.org/10.1021/acs.nanolett.0c02285.
9. L.P. Gor'kov and E.I. Rashba, Superconducting 2d system with lifted spin degeneracy: mixed singlet-triplet state. *Phys. Rev. Lett. Rev. Lett.* 87(3), 037004 (2001). https://doi.org/10.1103/PhysRevLett.87.037004.
10. S. Hoshino, R. Wakatsuki, K. Hamamoto and N. Nagaosa, Nonreciprocal charge transport in two-dimensional noncentrosymmetric superconductors. *Phys. Rev. B* 98(5), 054510 (2018). https://doi.org/10.1103/PhysRevB.98.054510.
11. S. Kanasugi and Y. Yanase, Multiorbital ferroelectric superconductivity in doped SrTiO3. *Phys. Rev. B* 100(9), 094504 (2019). https://doi.org/10.1103/PhysRevB.100.094504.
12. F. Ando, Y. Miyasaka, T. Li, J. Ishizuka, T. Arakawa, Y. Shiota, T. Moriyama, Y. Yanase and T. Ono, Observation of superconducting diode effect. *Nature* 584(7821), 373–376 (2020). https://doi.org/10.1038/s41586-020-2590-4.
13. E.G. Arnault, A.H. Al-Tawhid, S. Salmani-Rezaie, D.A. Muller, D.P. Kumah, M.S. Bahramy, G. Finkelstein and K. Ahadi,

Anisotropic superconductivity at KTaO3(111) interfaces. *Sci. Adv.* 9(7), eadf1414 (2023). https://doi.org/10.1126/sciadv.adf1414.
14. J.O. Dimmock, I. Melngailis and A.J. Strauss, Band structure and laser action in PbxSn1-xTe. *Phys. Rev. Lett.* 16(26), 1193–1196 (1966). https://doi.org/10.1103/PhysRevLett.16.1193.
15. J.S. Melvin and D.C. Hendry, Self-consistent relativistic energy bands for tin telluride. *J. Phys. C Solid State Phys.* 12(15), 3003 (1979). https://doi.org/10.1088/0022-3719/12/15/009.
16. O.N. Nashchekina, E.I. Rogacheva, A.I. Fedorenko, A.P. Isakina and A.I. Prokhvatilov, Low-temperature lattice instability in SnTe. *Low Temp. Phys.* 25(4), 285–289 (1999). https://doi.org/10.1063/1.593732.
17. P.B. Littlewood, The crystal structure of IV-VI compounds. II. A microscopic model for cubic/rhombohedral materials. *J. Phys. C Solid State Phys.* 13(26), 4875–4892 (1980). https://doi.org/10.1088/0022-3719/13/26/010.
18. T. Suski, M. Konczykowski, M. Leszczynski, D. Lesueur and J. Dural, Ferroelectric phase transition in electron irradiated PbSnTe crystals. *J. Phys. C Solid State Phys.* 15(27), L953 (1982). https://doi.org/10.1088/0022-3719/15/27/001.
19. M. Inoue, H. Kun Fun, H. Yagi and T. Tatsukawa, Spin resonance studies on structural phase transition in SnTe crystals. *J. Phys. Soc. Jpn.* 50(2), 353–354 (1981). https://doi.org/10.1143/JPSJ.50.353.
20. T.H. Hsieh, H. Lin, J. Liu, W. Duan, A. Bansil and L. Fu, Topological crystalline insulators in the SnTe material class. *Nat. Commun.* 3(1), 982 (2012). https://doi.org/10.1038/ncomms1969.
21. Y. Tanaka, T. Shoman, K. Nakayama, S. Souma, T. Sato, T. Takahashi, M. Novak, K. Segawa and Y. Ando, Two types of Dirac-cone surface states on the (111) surface of the topological crystalline insulator SnTe. *Phys. Rev. B* 88(23), 235126 (2013). https://doi.org/10.1103/PhysRevB.88.235126.
22. Y. Tanaka, Z. Ren, T. Sato, K. Nakayama, S. Souma, T. Takahashi, K. Segawa and Y. Ando, Experimental realization of a topological crystalline insulator in SnTe. *Nat. Phys.* 8(11), 800–803 (2012). https://doi.org/10.1038/nphys2442.
23. J.K. Hulm, C.K. Jones, D.W. Deis, H.A. Fairbank and P.A. Lawless, Superconducting interactions in tin telluride. *Phys. Rev.* 169(2), 388–394 (1968). https://doi.org/10.1103/PhysRev.169.388.
24. A.S. Erickson, J.-H. Chu, M.F. Toney, T.H. Geballe and I.R. Fisher, Enhanced superconducting pairing interaction in indium-doped tin telluride. *Phys. Rev. B* 79(2), 024520 (2009). https://doi.org/10.1103/PhysRevB.79.024520.
25. R.D. Zhong, J.A. Schneeloch, X.Y. Shi, Z.J. Xu, C. Zhang, J.M. Tranquada, Q. Li and G.D. Gu, Optimizing the superconducting transition temperature and upper critical field of Sn1-xInxTe. *Phys. Rev. B* 88(2), 020505 (2013). https://doi.org/10.1103/PhysRevB.88.020505.
26. R. Zhong, J. Schneeloch, Q. Li, W. Ku, J. Tranquada and G. Gu, Indium substitution effect on the topological crystalline insulator family (Pb1−xSnx)1−yInyTe: topological and superconducting properties. *Crystals* 7(2), 55 (2017). https://doi.org/10.3390/cryst7020055.
27. N. Haldolaarachchige, Q. Gibson, W. Xie, M.B. Nielsen, S. Kushwaha and R.J. Cava, Anomalous composition dependence of the superconductivity in in-doped SnTe. *Phys. Rev. B* 93(2), 024520 (2016). https://doi.org/10.1103/PhysRevB.93.024520.
28. M. Masuko, R. Yoshimi, A. Tsukazaki, M. Kawamura, K.S. Takahashi, M. Kawasaki and Y. Tokura, Molecular beam epitaxy of superconducting Sn1-xInxTe thin films. *Phys. Rev. Mater.* 4(9), 091202 (2020). https://doi.org/10.1103/PhysRevMaterials.4.091202.
29. R. Yoshimi, M. Masuko, N. Ogawa, M. Kawamura, A. Tsukazaki, K.S. Takahashi, M. Kawasaki and Y. Tokura, Versatile electronic states in epitaxial thin films of (Sn-Pb-In)te: from topological crystalline insulator and polar semimetal to superconductor. *Phys. Rev. Mater.* 5(9), 094202 (2021). https://doi.org/10.1103/PhysRevMaterials.5.094202.
30. R.C. Sharma and Y.A. Chang, The Sn−Te (Tin-Tellurium) system. *Bull. Alloy Phase Diagr.* 7(1), 72–80 (1986). https://doi.org/10.1007/BF02874985.
31. G. Grabecki, K.A. Kolwas, J. Wróbel, K. Kapcia, R. Puźniak, R. Jakieła, M. Aleszkiewicz, T. Dietl, G. Springholz and G. Bauer, Contact superconductivity in In–PbTe junctions. *J. Appl. Phys.* 108(5), 053714 (2010). https://doi.org/10.1063/1.3475692.
32. B. Chang, K.E. Singer and D.C. Northrop, Indium contacts to lead telluride. *J. Phys. Appl. Phys.* 13(4), 715 (1980). https://doi.org/10.1088/0022-3727/13/4/024.
33. D.B. Haviland, Y. Liu and A.M. Goldman, Onset of superconductivity in the two-dimensional limit. *Phys. Rev. Lett.* 62(18), 2180–2183 (1989). https://doi.org/10.1103/PhysRevLett.62.2180.
34. H.M. Jaeger, D.B. Haviland, B.G. Orr and A.M. Goldman, Onset of superconductivity in ultrathin granular metal films. *Phys. Rev. B* 40(1), 182–196 (1989). https://doi.org/10.1103/PhysRevB.40.182.
35. V.F. Gantmakher and V.T. Dolgopolov, Superconductor-insulator quantum phase transition. *Phys-Uspekhi* 53(1), 1 (2010). https://doi.org/10.3367/UFNe.0180.201001a.0003.
36. M. Tinkham, Effect of fluxoid quantization on transitions of superconducting films. *Phys. Rev.* 129(6), 2413–2422 (1963). https://doi.org/10.1103/PhysRev.129.2413.
37. P.B. Allen and M.L. Cohen, Carrier-concentration-dependent superconductivity in SnTe and GeTe. *Phys. Rev.* 177(2), 704–706 (1969). https://doi.org/10.1103/PhysRev.177.704.
38. M. Novak, S. Sasaki, M. Kriener, K. Segawa and Y. Ando, Unusual nature of fully gapped superconductivity in in-doped SnTe. *Phys. Rev. B* 88(14), 140502 (2013). https://doi.org/10.1103/PhysRevB.88.140502.
39. W.L. McMillan, Transition temperature of strong-coupled superconductors. *Phys. Rev.* 167(2), 331–344 (1968). https://doi.org/10.1103/PhysRev.167.331.
40. F. Marsiglio and J.P. Carbotte, Strong-coupling corrections to bardeen-cooper-schrieffer ratios. *Phys. Rev. B* 33(9), 6141–6146 (1986). https://doi.org/10.1103/PhysRevB.33.6141.
41. R.A. Klemm, A. Luther and M.R. Beasley, Theory of the upper critical field in layered superconductors. *Phys. Rev. B* 12(3), 877–891 (1975). https://doi.org/10.1103/PhysRevB.12.877.
42. T. Schumann, L. Galletti, H. Jeong, K. Ahadi, W.M. Strickland, S. Salmani-Rezaie and S. Stemmer, Possible signatures of mixed-parity superconductivity in doped polar $SrTiO_3$ films. *Phys. Rev. B* 101(10), 100503 (2020). https://doi.org/10.1103/PhysRevB.101.100503.
43. A.H. Al-Tawhid, S.J. Poage, S. Salmani-Rezaie, A. Gonzalez, S. Chikara, D.A. Muller, D.P. Kumah, M.N. Gastiasoro, J. Lorenzana and K. Ahadi, Enhanced critical field of superconductivity at an oxide interface. *Nano Lett.* 23(15), 6944–6950 (2023). https://doi.org/10.1021/acs.nanolett.3c01571.
44. J. Ruhman, V. Kozii and L. Fu, Odd-parity superconductivity near an inversion breaking quantum critical point in one dimension. *Phys. Rev. Lett.* 118(22), 227001 (2017). https://doi.org/10.1103/PhysRevLett.118.227001.
45. K. Dunnett, A. Narayan, N.A. Spaldin and A.V. Balatsky, Strain and ferroelectric soft-mode induced superconductivity in strontium titanate. *Phys. Rev. B* 97(14), 144506 (2018). https://doi.org/10.1103/PhysRevB.97.144506.
46. N.F.Q. Yuan and L. Fu, Supercurrent diode effect and finite-momentum superconductors. *Proc. Natl. Acad. Sci.* 119(15), e2119548119 (2022). https://doi.org/10.1073/pnas.2119548119.

47. M.N. Gastiasoro, M.E. Temperini, P. Barone and J. Lorenzana, Theory of superconductivity mediated by Rashba coupling in incipient ferroelectrics. *Phys. Rev. B* 105(22), 224503 (2022). https://doi.org/10.1103/PhysRevB.105.224503.
48. C. Setty, M. Baggioli and A. Zaccone, Superconducting dome in ferroelectric-type materials from soft mode instability. *Phys. Rev. B* 105, L020506 (2022). https://journals.aps.org/prb/abstract/10.1103/PhysRevB.105.L020506.
49. S.J. Poage, X. Gao, M. Baksi, S. Salmani-Rezaie, D.A. Muller, D.P. Kumah, C.N. Lau, J. Lorenzana, M.N. Gastiasoro and K. Ahadi, Violation of Pauli limit at KTaO3(110) interfaces. (2025). https://arxiv.org/abs/2502.13264.
50. A.H. Al-Tawhid, R. Sun, A.H. Comstock, D.P. Kumah, D. Sun, K. Ahadi, Spin-to-charge conversion at $KTaO_3$(111) interfaces. *Appl. Phys. Lett* 126, 091601 (2025). https://doi.org/10.1063/5.0247001.